Boosting the Efficiency of Quasi-2D Perovskites Light-emitting D iodes by Using Encapsulation Growth Method

Yanliang Liu [ab], Zhongkai Yu [a], Shi Chen [b], Jong Hyun Park [c], Eui Dae Jung [c], Seungjin Lee [d], Keehoon Kang [e], Seo-Jin Ko [f], Jongchul Lim [gh], Myoung Hoon Song [c], Baomin Xu[b]*, Henry J. Snaith [g], Sung Heum Park [a]*, and Bo Ram Lee [a]*

[a] Department of Physics, Pukyong National University, Busan 48513, Republic of Korea

[b] Department of Materials Science and Technology and Academy for Advanced Interdisciplinary Studies, Southern University of Science and Technology, Shenzhen, Guangdong Province 518055, China

[c] School of Materials Science and Engineering, Ulsan National Institute of Science and Technology (UNIST), UNIST-gil 50, Eonyang-eup, Ulsan 44919, Republic of Korea

[d] Department of Electrical and Computer Engineering, University of Toronto, 10 King's College Road, Toronto, Ontario, M5S 3G4, Canada

[e] Department of Physics and Astronomy, Seoul National University, Seoul 08826, Republic of Korea

[f] Division of Advanced Materials, Korea Research Institute of Chemical Technology (KRICT), Daejeon, 34114 Republic of Korea

[g] Clarendon Laboratory, Department of Physics, University of Oxford, Parks Road, Oxford, OX1 3PU, United Kingdom

[h] Graduate School of Energy Science and Technology, Chungnam National University, 99 Daehak-ro, Yuseong-gu, Daejeon, 34134, Republic of Korea

*Corresponding authors. E-mail: xubm@sustech.edu.cn (Baomin Xu); spark@pknu.ac.kr, (Sung Heum Park) and brlee@pknu.ac.kr (Bo Ram Lee)

Abstract

The fabrication of perovskite film is crucial for achieving efficient perovskite photoelectric device. Herein, a simple and novel encapsulation growth method was applied to prepare high-quality quasi-2D perovskite films with advantages of compact and uniform morphology, high crystallinity with lower defect density, enhanced photoluminescence quantum yield (PLQY) and optimized multidimensional domain distribution and crystallite orientation for perovskite light-emitting diodes (PeLEDs). The encapsulation growth method was found to decrease the proportion of the low-dimensional (n=1,2,3) domains while increasing the high-dimensional domains content with randomly-oriented crystals, which simultaneously enhanced the overall energy landscape effect and charges transport within the quasi-2D perovskite films, and the PLQY of the quasi-2D perovskites significantly improved from 9.2% to 60.0%. Finally, an efficient flexible green PeLEDs was obtained with a high luminous efficiency (LE) of 47.1 cd/A, and a luminance brightness of 8,300 cd/m^2, and an efficient sky-blue PeLEDs was also achieved with record EQE of 12.8 % by using encapsulation growth method. This encapsulation growth method provides a promising strategy for boosting the efficiency of quasi-2D PeLEDs.

Keywords: quasi-2D perovskites, encapsulation growth, charges transport, energy transfer, light-emitting diodes.

1. Introduction

Organic-inorganic halide perovskite materials have been demonstrated as a promising candidate for light-emitting diodes (PeLEDs) owing to their excellent optoelectronic properties, such as high photoluminescence quantum yields (PLQYs), color tunability over a wide-range by simply modulating the elemental composition, and a high color purity with a narrow full width at half-maximum emission (<20 nm) [1-8]. At present, efficient red and green PeLEDs with high external quantum efficiencies (EQEs) of over 20% have been achieved [9-11], which is comparable with state-of-the-art organic and quantum-dot LEDs. In contrast, the blue PeLEDs that are important for display and lighting application exhibit much lower efficiency with EQE around 10% [12-14]. In addition, flexible PeLEDs have gained attention in realizing ultrathin, light weight, highly conformable and nonfragile vivid displays [15-19]. Perovskite films can be prepared by low temperature solution-processing, which enables solvent-processed fabrication of flexible PeLEDs with advantages of low-cost and mass productivity [20-22].

Quasi-2D Ruddlesden-Popper (RP) halide perovskites produced by precursor-mixtures that contain bulky organic spacer cation and A-site cation of halide perovskites ABX_3 (X=Cl, Br, I) have been widely used as an active layer in efficient PeLEDs. In the solvent-processed preparation of perovskite films, anti-solvent washing methods have been proven to promote a rapid and uniform

nucleation of perovskites crystals by immediately washing out precursor solvents, resulting in the formation of smooth and full-coverage perovskite films [23,24], However, the fast crystallization inevitably introduce unintended defects [25-30], such as structural disorders, crystallographic defects, grain boundaries, and undesired phase mixtures owing to the incomplete growth of perovskite crystals within a short formation time. The defects create trap states, resulting in trap-mediated non-radiative recombination loss [31-33], which deteriorates the optoelectronic performance of PeLEDs. The quasi-2D perovskite films deposited by solvent-dropping methods possess a mixture of multiple dimensional domains (n=1,2,3,4,5⋯) [3,34], and the quasi-2D perovskite domains are found to preferentially orient parallel to the substrate [35,36]. Therefore, an excessive content of low-dimensional (n=1,2,3) domains can form a higher density of bulky insulating organic spacers within the charges transport pathways, which impedes the charge transport in the quasi-2D perovskite films [37,38]. In addition, tailoring the distribution of multiple-dimensional domains can yield a gradient energy landscape in quasi-2D perovskites, that enables efficient energy transfer from low-dimensional domains to high-dimensional radiative domains [34,39], which is crucial for achieving high PLQY and LED performance. It is well known that perovskite crystal growth is significantly influenced by deposition methods [23,40-45], and controlling the residual solution (DMF,DMSO) evaporation rate in perovskite precursor films during annealing is an efficient strategy to promote perovskite crystal growth [46, 47]. However, the perovskite crystal growth usually

leads to a rough surface with a reduced film-coverage, which decreases the device performance [48]. Therefore, the development of effective methods that enable the control growth of highly crystalline perovskites is a promising strategy to achieve high-quality perovskite emitting layers for improving the performance of PeLEDs.

In this study, we report an encapsulation growth method to fabricate high-quality quasi-2D perovskite film, which is produced by simply shielding a scotch tape on perovskite precursor film during annealing. The top scotch tape can contain the residual solution in perovskite precursor film, thus promoting the growth of quasi-2D $(PMA)_2Cs_{n-1}Pb_nBr_{3n+1}$(n=3) perovskites with low crystal defects, and its PLQY significantly improved from 9.2% to 60.0%. Moreover, due to the space limitation between the substrate and the top scotch tape during the film formation, the resulting perovskite film exhibits a uniform and compact morphology. More interestingly, the encapsulation growth was found able to decrease the proportion of low-dimensional (n=1,2,3) domains, while increasing the proportion of high-dimensional domains with randomly crystal orientation, and thereby tailoring the energy landscape in the quasi-2D perovskites, that yields an efficient charge transport and energy transfer to the lowest-bandgap perovskite radiative domains. Using the encapsulation growth of quasi-2D $(PMA)_2Cs_{n-1}Pb_nBr_{3n+1}$(n=3) perovskite films, an efficient flexible green PeLEDs was achieved with a high luminous efficiency of 47.1 cd/A, and luminance of 8,300 cd/m^2, and an ITO-free flexible PeLEDs with a PEDOT:PSS anode was also fabricated with a luminous efficiency of 20.6 cd/A, and

luminance of 1,900 cd/m^2, and their flexibility was studied by empirical cyclic bending test with various bending radii. Moreover, an efficient flexible sky-blue PeLEDs based on quasi-2D perovskites (PEACl:$CsPbBr_3$=1:1, YCl_3 2%), emitting at 493 nm, was also achieved with a record EQE of 12.8% by using the encapsulation growth method. The encapsulation growth of quasi-2D perovskite films is an effective method for boosting the efficiency of PeLEDs.

2. Results and Discussion

In the solvent-based fabrication of perovskite film, a fast crystallization is essential for achieving a compact and uniform film morphology. However, the fast crystallization inevitably creates detrimental defects and undesired phase mixtures in perovskites. According to our previous study, controlling the evaporation speed of residual solvent in perovskite precursor film is an efficient strategy to facilitate the perovskite crystal growth with a reduced defects density [46,49,50]. Base on this, herein, an encapsulation growth method was used to deposit high-quality quasi-2D perovskite films for efficient PeLEDs as shown in Figure 1(a). A scotch tape was tightly pasted on top of a quasi-2D $(PMA)_2Cs_{n-1}Pb_nBr_{3n+1}$(n=3) perovskite precursor film on a flexible PEN substrate during annealing. The scotch tape can encapsulate the quasi-2D perovskite precursor film and contain the residual DMSO solution for a long time, thus providing enough time for high-quality growth of quasi-2D perovskites. In addition, due to an excellent flexibility of both the PEN substrate and scotch tape, the scotch tape is able to fully attach to the top surface of the perovskite

film sandwiched between the flexible substrate and scotch tape. Due to the space-confined growth process, the perovskite material growth occurs parallel to the substrate, leading to a uniform and compact film morphology with a low RMS value of 3.34 nm as shown in Figure S1.

Figure 1 (b) shows an image of $(PMA)_2Cs_{n-1}Pb_nBr_{3n+1}$(n=3) perovskite film with a half of the film made by the encapsulation growth method (right) and the other half with the conventional method (left). The right side was covered by a scotch tape during annealing at 100 ℃ for 10 min, in order to induce the encapsulation growth of the crystals. As we can see, the region of the film made by the encapsulation growth method clearly appears to exhibit a brighter green emission than the region of the film deposited by the conventional method when illuminated under UV light, and its PLQY was increased from 9.2% to 60.0% by using the encapsulation growth method as shown in Figure 1 (c), which would contribute to efficient PeLEDs, as discussed later. For further investigating the effect of the encapsulation growth method on the PL intensity of the quasi-2D perovskite films, we used para-film and glass sheet to shield the perovskite film, respectively, as shown Figure S2, the para-film and glass sheet assisted encapsulation growth of perovskite films also results in an enhanced PL compared to the reference film.

The UV-Visible absorption spectrum of quasi-2D $(PMA)_2Cs_{n-1}Pb_nBr_{3n+1}$(n=3) perovskite films made by conventional method (denoted as “conventional perovskites” from here) exhibits several peaks that correspond to multiple dimensional domains

(n=1,2,3…) as shown in Figure 1 (d), which is consistent with previous reports [2], and the quasi-2D multilayered perovskite films actually comprised multiple-dimensional perovskite domains (with various n values from 1,2,3 and 4 to near ∞) centered on an average value n [51,52], and it creates bandgap alignment between perovskite domains with various n values, resulting in the internal energy transfer from wide-bandgap low-dimensional domains to low-bandgap high-dimensional domains in quasi-2D perovskite films [2,3]. Spectacularly, the peak intensities that correspond to n=1,2,3 low-dimensional domains decreased in the film made by the encapsulation growth method (denoted as "encapsulation growth perovskites" from here), which indicates the decreased proportion of the low-dimensional domains (n=1,2,3), while exhibiting an enhanced absorbance at a near band-edge with a noticeable red-shift, which indicates an increased proportion of low-bandgap, high-dimensional domains in the encapsulation growth quasi-2D perovskites. This would be beneficial for the charge transport in the quasi-2D perovskites. The observed changes of multiple dimensional domain distribution in the encapsulation growth quasi-2D perovskite films might be tentatively assigned to the shielding effect of the top scotch tape, which is able to hold the residual DMSO solution for a long time, thus promoting the 3D perovskites phase growth [53,54], which results in an increased proportion of high-dimensional domains and simultaneously decreased low-dimensional domains in quasi-2D perovskite film. In addition, according to previous reports, the nucleating position of crystal domains

within the solution phase during the film deposition is important for crystal orientation [55]. Therefore, the top scotch tape may also affect the quasi-2D perovskite crystal nucleation position and orientation.

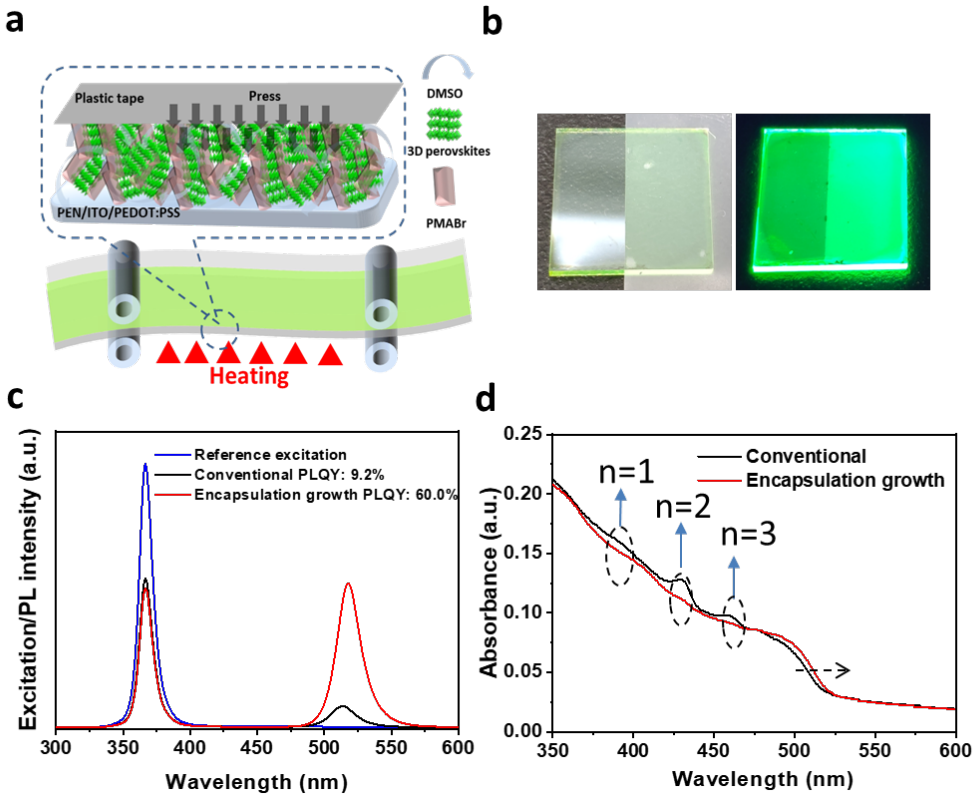

Figure 1. (a) Schematic diagrams for the encapsulation growth method of quasi-2D $(PMA)_2Cs_{n-1}Pb_nBr_{3n+1}$(n=3) perovskite films, (b) images of conventional and encapsulation growth perovskite films without (left) and with (right) UV lamp excitation, (c) Photoluminescence quantum yield (PLQY) and (d) UV-Visible absorption of conventional and encapsulation growth perovskites.

The effect of the encapsulation growth method on the quasi-2D $(PMA)_2Cs_{n-1}Pb_nBr_{3n+1}$(n=3) perovskite crystal was investigated by using grazing-incidence wide-angle X-ray scattering (GIWAXs). Figure 2 (a) exhibits the GIWAXs patterns of the convention quasi-2D perovskites, and it shows discrete

Bragg spots with crystal diffractions (100) and (200) at 1.05 and 2.10 Å, which indicates a preferential oriented crystal [56]. According to a previous study, the conventional quasi-2D perovskites with small n values ($n \leqslant 3$) mainly grew in in-plane orientation to the substrate and consequently formed multilayered RP-phase nanoplatelets as shown in the schematic illustration [36], which severely hinders the charge transport in the quasi-2D perovskite films. In contrast, the encapsulation growth quasi-2D perovskites exhibit a ring-like Debye Scherer pattern, indicating a randomly oriented crystal as shown in Figure 2 (b). The random orientation of the quasi-2D perovskites can effectively accelerate the charge transport in perovskite films through enhancing the contact between neighbouring perovskite crystals as shown in the schematic illustration of the encapsulation growth quasi-2D perovskites [37]. Moreover, the long-range lateral charge carrier mobility of quasi-2D perovskites was investigated by a horizontal transient photo-conductivity (TPC) measurement shown in Figure 2 (c) [57]. The conventional quasi-2D perovskites exhibited a higher lateral charge carrier mobility than the encapsulation growth quasi-2D perovskite, which is attributed to a in-plane crystal orientation of the conventional films. In contrast, as expected, the encapsulation growth quasi-2D perovskite shows enhanced electron and hole transport properties compared with the convention sample, which is beneficial for efficient PeLEDs. In particular, the encapsulation growth quasi-2D perovskites exhibits well-grown crystal grains that contain multiple dimensional domains as shown in the HR-TEM images in Figure S3, which enables the efficient

energy transfer form low dimensional domains to high dimensional domains in quasi-2D perovskites.

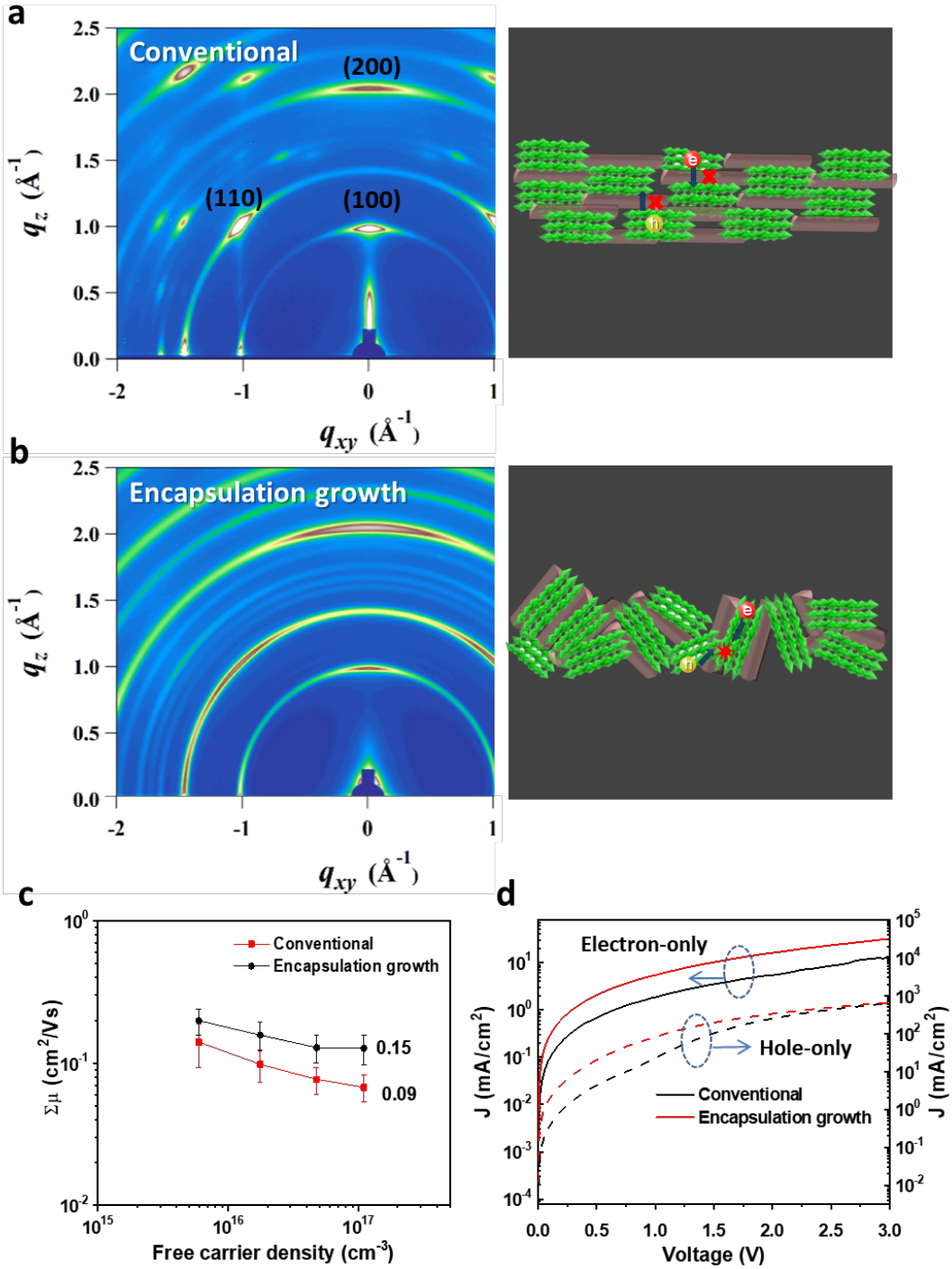

Figure 2. GIWAXs patterns and corresponding schematic illustrations of quasi-2D $(PMA)_2Cs_{n-1}Pb_nBr_{3n+1}$(n=3) perovskite films fabricated by (a) conventional and (b)

encapsulation growth method, (c) horizontal transient photo-conductivity of quasi-2D perovskite films and (d) J-V characteristics of electron-only and hole-only devices.

The ultrafast transient absorption (TA) measurement was conducted to monitor the energy transfer dynamics of photogenerated carriers in the conventional and encapsulation growth quasi-2D $(PMA)_2Cs_{n-1}Pb_nBr_{3n+1}$(n=3) perovskites. As shown in Figure 3 (a),(b), several distinctive ground-state bleach (GSB) peaks are observed, which is consistent with the UV-Visible absorption spectra of quasi-2D perovskites in Figure 1 (d). According the time-dependent TA spectra of quasi-2D perovskites in Figure 3 (a),(b), the low-dimensional (n=1,2,3) GSB peaks are firstly formed at 0.4 ps, after that, the high-dimensional GSB peak emerges at 1 ps, meanwhile the low-dimensional GSB peaks reduce. That indicates an energy transfer from the low-dimensional domains to dominated high-dimensional domains in quasi-2D perovskites as shown in Figure 3 (d). The energy migration completed in the first 5 ps while the high-dimension GSB peaks reached the maximum value. For further investigating the energy transfer in the conventional and encapsulation growth perovskites, we made the TA spectra of high-dimensional GSB peaks as a function of the delay time as shown in Figure 3(c). The encapsulation growth quasi-2D perovskites exhibits a faster improvement of GSB peak intensity than the conventional perovskites, indicating that an enhanced energy transfer, which may attribute to more-graded energy landscape due to the optimized multidimensional domain distribution in the encapsulation growth quasi-2D perovskites. The enhanced energy transfer is beneficial for outpacing the trapping and non-radiative

recombination losses in perovskites, resulting in the high PLQY of perovskites and improved PeLEDs device performance [39].

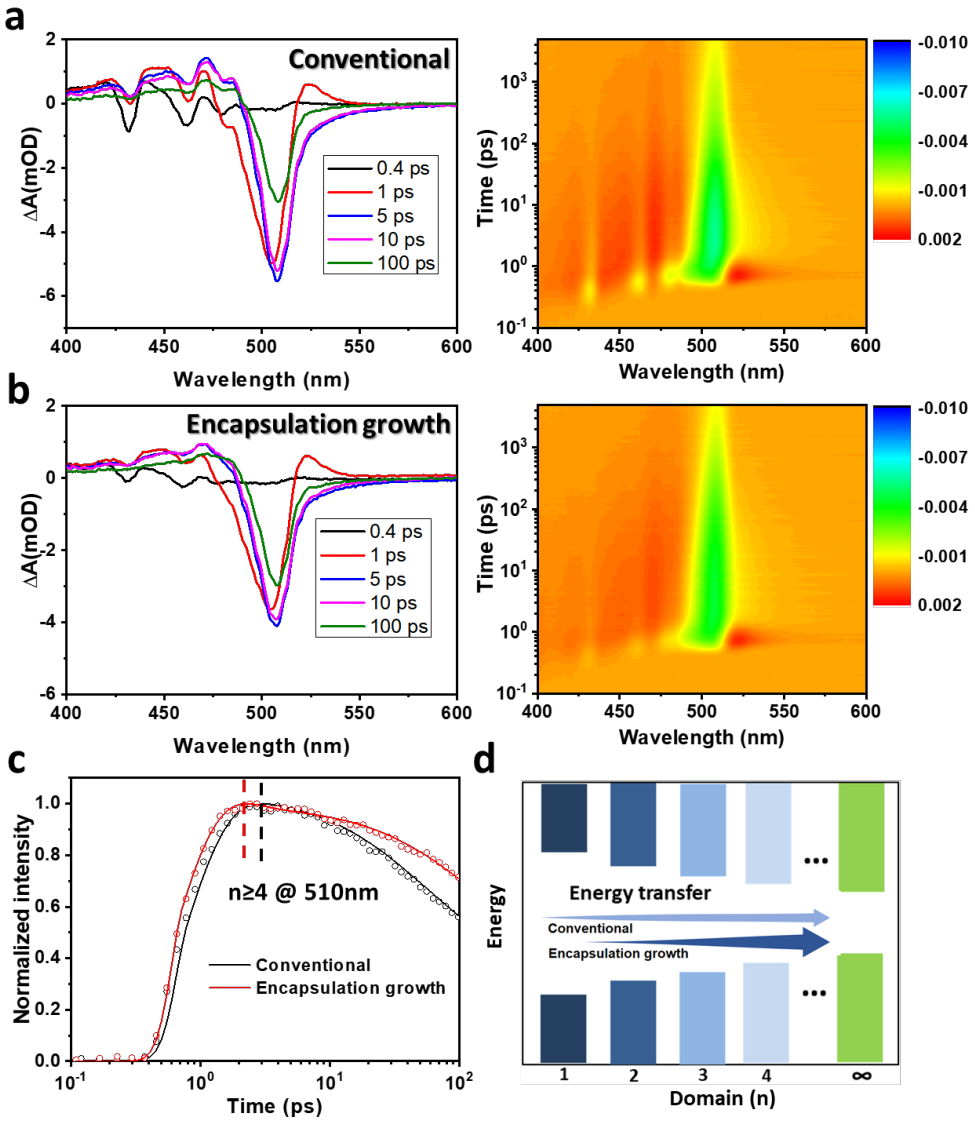

Figure 3. TA measurements for quasi-2D $(PMA)_2Cs_{n-1}Pb_nBr_{3n+1}$(n=3) perovskite film, (a), (b) TA spectra at selected timescales and time-wavelength-dependent TA color maps for the conventional and encapsulation growth quasi-2D perovskite films, (c) TA spectra at high-dimensional GSB peak as a function of delay time for the quasi-2D perovskite film, (d) Schematic illustration of energy transfer process in quasi-2D perovskites.

To study the photo-physical properties of the quas-2D $(PMA)_2Cs_{n-1}Pb_nBr_{3n+1}$(n=3) perovskite films, the steady-state photoluminescence (PL)

and time-resolved photoluminescence (TR-PL) of the conventional and encapsulation growth quasi-2D perovskite films on quartz substrate were measured as shown in Figure 4 (a) and (b). The encapsulation growth perovskite film exhibits a significantly higher PL intensity than the conventional sample. In normal condition, the crystal defects in perovskite materials can act as charges trap sites, resulting in a decreased PL intensity. Therefore, the higher PL intensity indicates a lower defect density in the encapsulation growth perovskites in contrast to the conventional sample. Moreover, the full width at half maximum (FWHM) of PL spectrum of quasi-2D perovskite films obviously decreased from 23.6 nm to 21.4 nm by using the encapsulation growth method, that can also be attributed to the reduced defect density in perovskite crystals [58,59]. In addition, the encapsulation growth perovskite film exhibits a red-shifted maximum PL peak, that may be attributed to a change in the distribution of different n domains (i.e. an increased proportion of low bandgap high-n domains and a decreased proportion of high-bandgap low-n domains in the encapsulation growth quasi-2D perovskites, which is consistent with the UV-Visible absorption spectra in Figure 1 (d)).

The TR-PL of quasi-2D $(PMA)_2Cs_{n-1}Pb_nBr_{3n+1}$(n=3) perovskites was fitted with a bi-exponential decay, where the A_1 and A_2 are the fractional contributions of the PL decay lifetime, and short lifetime (τ_1) corresponds to a fast decay process related to quenching (including charge transfer) and defects, and the long lifetime (τ_2) corresponds to the slower decay related to recombination, as shown in Figure 4 (b).

The conventional quasi-2D perovskites exhibit a short lifetime $\tau_1 = 1.00$ ns and a long lifetime $\tau_2 = 10.87$ ns, in contrast, the encapsulation growth quasi-2D perovskites shows a significantly improved short lifetime $\tau_1 = 5.91$ ns and long lifetime $\tau_2 = 59.22$ ns. The τ_{ave} of quasi-2D perovskite films obviously improved form 7.92 ns to 47.55 ns by using the encapsulation growth method, which indicates a reduced defect density and enhanced carrier transport. The PL decay parameters are summarized in Table S1. The confocal PL images of the encapsulation growth perovskite films exhibit a brighter PL emission with significantly reduced dark spots that may act as charges trap site compared with the conventional perovskite film, as shown in figure 4 (c), which is consistent with the PL and TR-PL results. This result indicates that the encapsulation growth method can effectively improve the crystal quality and optical properties of quasi-2D perovskite materials.

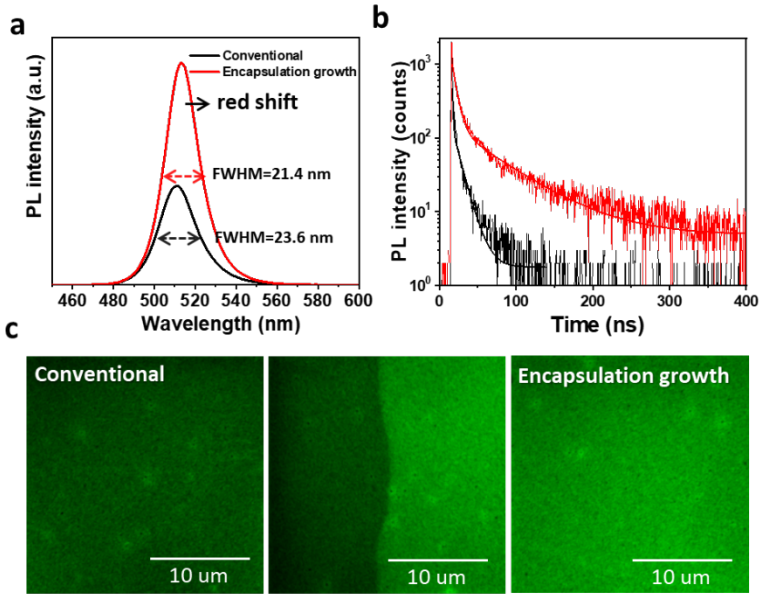

Figure 4. (a) Steady-state PL and (b) time-resolved PL spectra of the conventional and encapsulation growth quasi-2D $(PMA)_2Cs_{n-1}Pb_nBr_{3n+1}$(n=3) perovskite films. (c)

confocal PL images of the conventional and encapsulation growth quasi-2D perovskite films.

We fabricated flexible green PeLEDs with the quasi-2D $(PMA)_2Cs_{n-1}Pb_nBr_{3n+1}$(n=3) perovskite films deposited by the conventional and encapsulation growth method with the device configuration of PEN/ITO/PEDOT:PSS (Al4083)/quasi-2D perovskites/TPBi/LiF/Al, and examined their device performance. The current density-voltage (J-V), luminance-voltage (L-V), luminous efficiency-voltage (LE-V) and electroluminescence (EL) curves of the conventional and encapsulation growth PeLEDs are shown in Figure 5 (a-d), respectively. The summarized device performance parameters are displayed in Table 1. The encapsulation growth PeLEDs shows a smaller leakage current at a low bias voltage form 0 to 3V, as shown in Figure 5 (a), which may be attribute to the compact and uniform morphology of encapsulation growth perovskite film. As shown in Figure 5 (b), the encapsulation growth PeLEDs exhibit a lower operating voltage and higher luminance, that may correspond to the enhanced charges transport properties and an efficient radiative recombination of electrons and holes due to a lower defect intensity and higher quality quasi-2D perovskite films. The encapsulation growth flexible PeLEDs shows an excellent device performance with the maximum luminance of 8,300 cd/m^2, and a high luminous efficiency of 47.1 cd/A. The encapsulation growth PeLEDs exhibits a significantly higher EL intensity than the conventional device with a slightly red shifted luminescence peak, which is consistent with the PL spectra of the conventional and encapsulation growth quasi-2D perovskite materials in Figure 4

(a). The EL intensity of the encapsulation growth PeLEDs gradually increases as the bias voltage is increased without any changes in the peak position as shown in Figure 5 (e). Figure 5 (f) shows the impedance spectra (Nyquist plots) of the conventional and encapsulation growth PeLEDs, which was used to extract the internal resistance of the devices. The encapsulation growth PeLEDs exhibits a smaller semicircle than the conventional device, representing the decreased device internal resistance. That results in the lower operating voltage of the encapsulation growth PeLEDs compared to the conventional PeLEDs.

It is well known that ITO film is brittle, and therefore it is not readily applicable in highly flexible PeLEDs. For further improving the flexibility of PeLEDs, an ITO-free flexible PeLEDs were fabricated with the device configuration of PEN/PEDOT:PSS(Ph1000) /quasi-2D perovskites/TPBi/LiF/Al. The PEDOT:PSS(Ph1000) instead of ITO works as an anode in PeLEDs, and it has an excellent transmittance of 89.7% at 516 nm as show in Figure S4. The ITO-free encapsulation growth PeLEDs also exhibits a high device performance with the maximum brightness of 1,900 cd/m^2, and an excellent LE of 20.6 cd/A, and it also shows a smaller leakage current and lower operating voltage compared to the conventional device as shown in Figure 5 (g-i). In addition, the flexibility of the ITO-based and ITO-free encapsulation growth PeLEDs were measured through an empirical cyclic bending test. Figure S5 shows the device configuration and photographs of ITO-free PeLEDs under various bending radii (R_b) (values of 10, 5, 1

mm) to confirm the cyclic bending condition. The ITO-based PeLEDs exhibits a fast decrease of luminance in the R_b of 10 mm in the cyclic bending test. In contrast, the luminance of ITO-free PeLEDs with R_b of 10 and 5 mm bending conditions maintain 90 % and 64 % percent of their initial luminance after 400 bending cycles, while the device with the bending R_b of 1 mm losses 85 % percent of its initial luminance after only 100 bending cycles. The sharp reduction of luminance of PeLEDs may be caused by the mechanical breakdown of perovskites materials due to its brittle crystal structure [15], and the critical bending radius of flexible PeLEDs is around on the order of 1 mm.

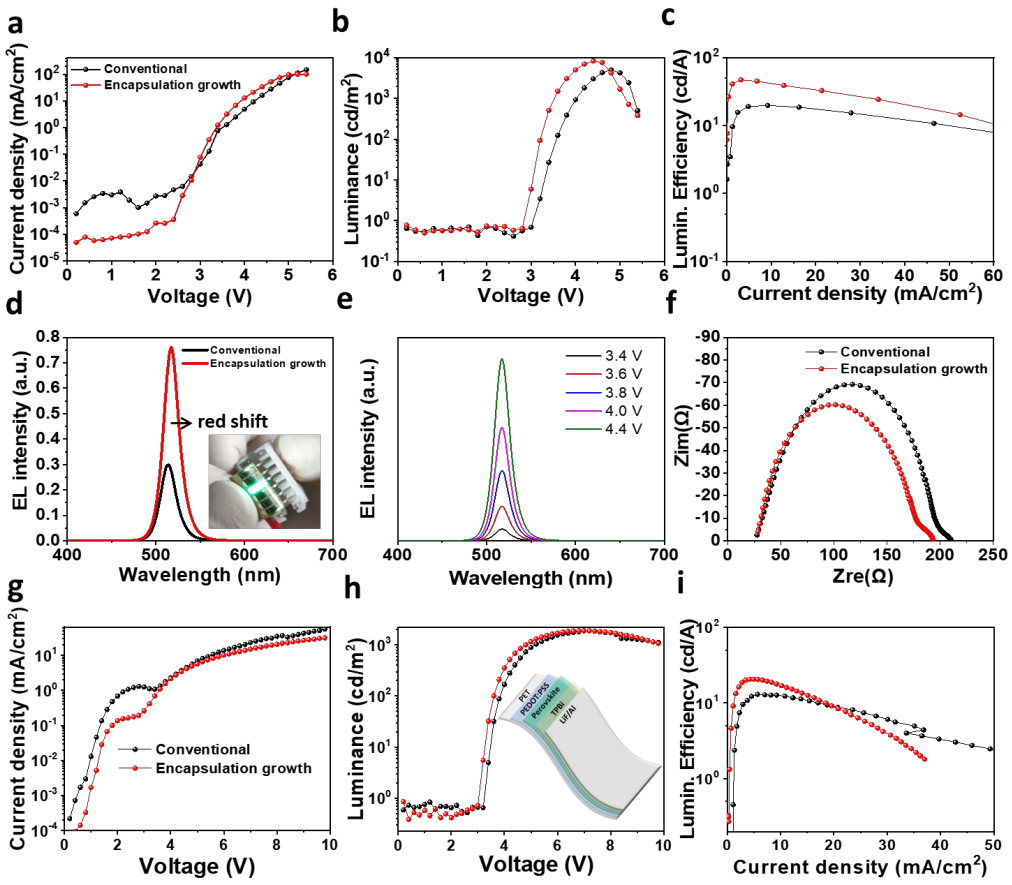

Figure 5. (a) J-V, (b) L-V, (c) LE-J and (d) EL spectrum, curves of conventional and encapsulation growth flexible green PeLEDs. (e) EL spectrum of encapsulation

growth PeLEDs at various applying voltage. (f) impedance spectra of PeLEDs. (g) J-V, (h) L-V, (i) LE-J curves of ITO-free flexible green PeLEDs

Table 1. Device performance of flexible PeLEDs.

Device	L_{max} [cd/m^2]@bias	CE_{max} [cd/A]@bias	Operating Voltage [V]
Conventional	5000@4.8	19.8@4.2	3.2
Encapsulation growth	8300@4.4	47.1@3.6	3.0
Conventional (ITO-free)	1910@11.4	13.0@10.5	3.4
Encapsulation growth (ITO-free)	1900@7.8	20.6@5.1	3.2

For further investigating the effect of encapsulation growth method on quasi-2D perovskites crystal growth, a sky-blue emission (PEACl:$CsPbBr_3$=1:1, YCl_3 2%) quasi-2D perovskite film was also fabricated as shown in Figure 6 (a). The encapsulation growth perovskite film exhibits a clearly enhanced blue emission with the main PL emission peak located at 495 nm. In contrast, the conventional perovskite film shows a low PL emission with multiple emission peaks, which indicates a multiple dimensional domain distribution and inefficient energy transfer in the conventional quasi-2D perovskite film. The encapsulation growth perovskite film also exhibits a significantly longer PL lifetime than the conventional sample as shown in Figure 6 (b), which is consistent with a preceding $(PMA)_2Cs_{n-1}Pb_nBr_{3n+1}$ (n=3)

quasi-2D perovskite film prepared by the encapsulation growth method. Subsequently, an efficient sky-blue PeLEDs based on (PEACl:$CsPbBr_3$=1:1, YCl_3 2%) quasi-2D perovskite film with the device configuration of glass-ITO/PEDOT:PSS/PVK/quasi-2D perovskites/TPBi/LiF/Al was fabricated as shown in Figure S6. Figure 6 (c-f) show the J-V, LE-V, EL and EQE-V curves of the the sky-blue PeLEDs. The encapsulation growth sky-blue PeLEDs shows a reduced leakage current and improved device efficiency with the maximum luminance of 6,600 cd/m^2, which is almost the same with the preceding flexible green PeLEDs. The device exhibits a stable sky-blue emission with 493 nm emission peak at various applied voltages. The EQE of the sky-blue PeLEDs significantly improved from 4.5% to 12.8% by using the encapsulation growth method. In summary, the encapsulation growth method can be extended to fabricate various high-quality quasi-2D perovskite fsilm with different precursor compositions and emission light wavelengths for improving the device performance of quasi-2D PeLEDs.

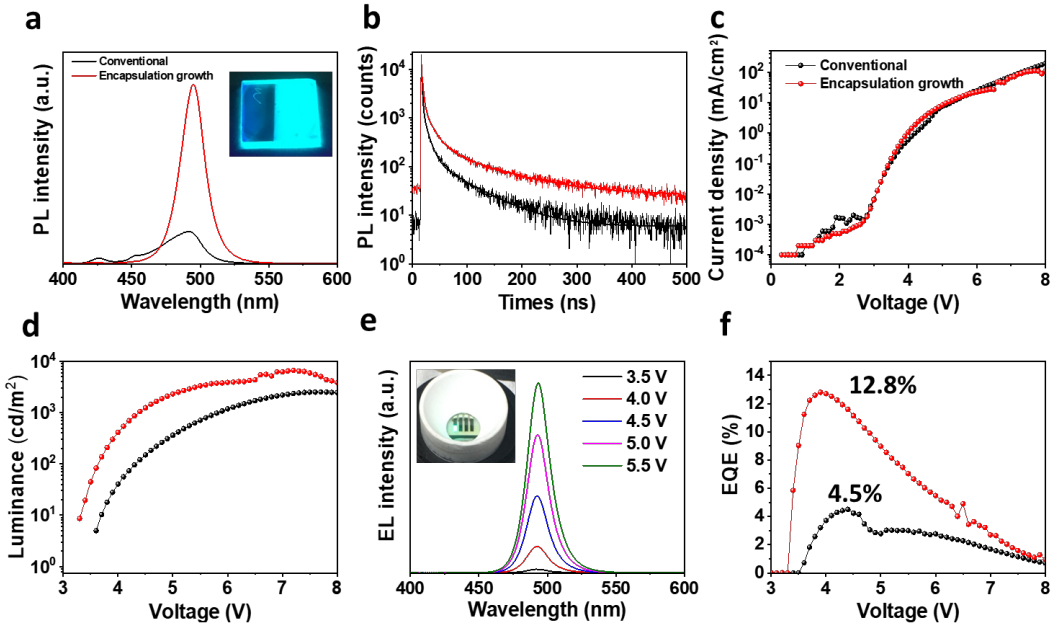

Figure 6. (a) Steady-state PL (insert: images of conventional (left) and encapsulation growth (right) quasi-2D (PEACl:$CsPbBr_3$=1:1, YCl_3 2%) perovskite film under UV lamp excitation) and (b) time-resolved PL spectra of the conventional and encapsulation growth quasi-2D perovskite films, (c) J-V, (d) L-V, (e) EL and (f) EQE-V curves of sky-blue PeLEDs.

3. Conclusion

In conclusion, we demonstrated an encapsulation growth method to prepare high-quality quasi-2D perovskite films for PeLED application, and it provides an excellent combination of structural and photophysical properties of quasi-2D $(PMA)_2Cs_{n-1}Pb_nBr_{3n+1}$(n=3) perovskite films, including a compact and uniform film morphology with a low RMS value of 3.34 nm, enhanced crystallinity with a low density defects, a high photoluminescence quantum yield (PLQY) and optimized multidimensional domain distribution. The encapsulation growth method provides enough time for the quasi-2D perovskite crystal growth to occur and the PLQY of

quasi-2D perovskites significantly improved from 9.2% to 60.0%. More interestingly, the encapsulation growth method was found to tailor the distribution of the multi-dimensional domains with a reduced proportion of low-dimensional domains and an increased proportion of high-dimensional domains, leading to a more-graded energy landscape in the quasi-2D perovskite films, that facilitate an efficient charge transport and energy transfer to the lowest-bandgap perovskite radiative domains. Finally, efficient flexible green PeLEDs based on the encapsulation growth quasi-2D $(PMA)_2Cs_{n-1}Pb_nBr_{3n+1}$(n=3) perovskite emission layer was achieved with a high luminous efficiency of 47.1 cd/A, and a luminance of 8,300 cd/m^2, and an ITO-free flexible green PeLEDs with a PEDOT:PSS anode was also fabricated with a luminous efficiency of 20.6 cd/A, and a high luminance of 1,900 cd/m^2, and their flexibility were studied by empirical cyclic bending test. In addition, an efficient sky-blue PeLEDs based on (PEACl:$CsPbBr_3$=1:1, YCl_3 2%) quasi-2D perovskite films prepared by the encapsulation growth method also achieved a record EQE of 12.8 %. Therefore, we believe that the encapsulation growth technique developed in this work can be a tool for forming high-quality quasi-2D perovskite films with various compositions, and therefore leading to the development of high-performance quasi-2D PeLEDs.

4. Experimental Section

Materials: All solvents purchased from Sigma-Aldrich were used without further purification. n-butylammine bromide (PMABr), phenethylammonium chloride (PEACl), lead bromide ($PbBr_2$, 99.99%) and Cesium bromide (CsBr, 99.99%) were purchased from Tokyo Chemical Industry (TCI).

Device Fabrication: The flexible green PeLEDs were fabricated on an ITO-PEN substrate with device architecture of PEN/ITO/PEDOT:PSS(Al4083)/quasi-2D perovskites/TPBi/LiF/ Al. The ITO-glass substrate was cleaned and dried at 70 ^{o}C overnight. The PEDOT:PSS film was spin-casted on ITO at 4500 rpm for 40s and dried for 10 min at 140 ^{o}C in air, and then transferred into a glove box. The perovskite precursor (0.25M with $PbBr_2$, CsBr, and PMABr at a molar ratio of 1.5:1:1 in DMSO) solution was deposited on the substrate by spin-coating at speed of 5000 rpm for 15 s with instant chlorobenzene (CB) solvent cleaning during spinning. In conventional case, the perovskite precursor film was annealed at 100 ^{o}C for 10 min. In encapsulation growth, a scotch tape (3M) was closely pasted on perovskite precursor film, then, the sample was annealing at 100 ^{o}C for 10 min. After annealing, the scotch tape was peeled off from the sample, and the perovskite film was further annealed at 100 ^{o}C for 2 min to completely remove the remaining solvent. Finally, the TPBi (60 nm), LiF (1 nm) and Al (100 nm) was sequentially thermal deposited in 5×10-7 Torr vacuum. In the fabrication of ITO-free flexible green PeLEDs, a PEDOT:PSS(Ph1000) layer was spin-casted on PEN substrate at 5000 rpm for 40s and dried at 140 ^{o}C for 10 min in air. In the fabrication of sky-blue PeLEDs, the perovskite precursor (0.15M

PEACl:$CsPbBr_3$=1:1, YCl_3 2% in DMSO) solution was deposited on the substrate by spin-coating at speed of 5000 rpm for 15 s with instant chlorobenzene (CB) solvent cleaning during spinning, and the remaining fabrication steps is same with preceding flexible green PeLEDs.

Characterization: The XRD spectra, SEM image, AFM image, PL and TR-PL spectra of the quasi-2D perovskite films were characterized with our previously reported method [46,50]. The GIWAXS results were observed using X-rays (E = 19.0 keV and λ = 0.6530 Å). A 2D charge-coupled device (CCD) detector (MX225-HS, Rayonix L.L.C., USA) was used at a distance of 240.4 mm from the sample with a grazing incident angle of 0.128° and an exposure time of 60 s. The TEM images were performed on a Hitachi H-7500. The transient photo-conductivity of quasi-2D perovskite films was test according to previous study The confocal PL images were measured using an LSM 780 NLO laser scanning confocal microscope (Carl Zeiss) with a 100× oil immersion objective (a Plan-APO, NA = 1.46) with a 405 nm excitation diode laser. The EL spectra of the PeLEDs were measured using an SR-3AR spectrophotometer. The current J-V-L curves of the PeLEDs were measured using a Keithley 2450 source measure unit combined with a UVIS-50 spot photodetector. An impedance analyzer (1260 Impedance/Gain-Phase Analyzer, Solartron) was used to confirm the existence of the trap state of various samples. The EQE of the perovskite LED were recorded simultaneously by a commercialized system (XPQY-EQE, Guangzhou Xi Pu Optoelectronics Technology Co., Ltd.) that

was equipped with an integrated sphere (GPS-4P-SL, Labsphere) and a photodetector array (S7031-1006, Hamamatsu Photonics).

Acknowledgements

Y.L. Z.Y. and S.C contributed equally to this work. This study was supported by the National Research Foundation of Republic of Korea (NRF-2018R1C1B6005778 and 2020R1A2B5B01001611), and the Peacock Team Project funding from Shenzhen Science and Technology Innovation Committee (Grant No. KQTD20150331101823 70). This work was also financially supported by the National Natural Science Foundation of China (62004091, 62004089) and the Fundamental Research project from Shenzhen Science and Technology Innovation Committee (Grant No. JCYJ20190809150811504) and the Joint Funds project from Guangdong Basic and Applied Basic Research Fundation (Grant No. 2019A1515110439).

Reference

[1] H. Cho, S.-H. Jeong, M.-H. Park, Y.-H. Kim, C. Wolf, C.-L. Lee, J.H. Heo, A. Sadhanala, N. Myoung, S. Yoo, S.H. Im, R.H. Friend, T.-W. Lee, Science 350 (2015) 1222-1225.

[2] M. Yuan, L.N. Quan, R. Comin, G. Walters, R. Sabatini, O. Voznyy, S. Hoogland, Y. Zhao, E.M. Beauregard, P. Kanjanaboos, Z. Lu, D.H. Kim, E.H. Sargent, Nat. Nanotechnol. 11 (2016) 872-877.

[3] N. Wang, L. Cheng, R. Ge, S. Zhang, Y. Miao, W. Zou, C. Yi, Y. Sun, Y. Cao, R. Yang, Y. Wei, Q. Guo, Y. Ke, M. Yu, Y. Jin, Y. Liu, Q. Ding, D. Di, L. Yang, G. Xing, H. Tian, C. Jin, F. Gao, R.H.

Friend, J. Wang, W. Huang, Nat. Photonics 10 (2016) 699-704.
[4] Y.-H. Kim, H. Cho, J.H. Heo, T.-S. Kim, N. Myoung, C.-L. Lee, S.H. Im, T.-W. Lee, Adv. Mater. 27 (2015) 1248-1254.
[5] T. Chiba, Y. Hayashi, H. Ebe, K. Hoshi, J. Sato, S. Sato, Y.-J. Pu, S. Ohisa, J. Kido, Nat. Photonics 12 (2018) 681-687.
[6] L. Protesescu, S. Yakunin, M.I. Bodnarchuk, F. Krieg, R. Caputo, C.H. Hendon, R.X. Yang, A. Walsh, M.V. Kovalenko, Nano Lett. 15 (2015) 3692-3696.
[7] S. Lee, J.H. Park, Y.S. Nam, B.R. Lee, B. Zhao, D. Di Nuzzo, E.D. Jung, H. Jeon, J.-Y. Kim, H.Y. Jeong, R.H. Friend, M.H. Song, ACS Nano 12 (2018) 3417-3423.
[8] H. Huang, J. Raith, S.V. Kershaw, S. Kalytchuk, O. Tomanec, L. Jing, A.S. Susha, R. Zboril, A.L. Rogach, Nat. Commun. 8 (2017) 996.
[9] B. Zhao, S. Bai, V. Kim, R. Lamboll, R. Shivanna, F. Auras, J.M. Richter, L. Yang, L. Dai, M. Alsari,X.J. She, L. Liang, J. Zhang, S. Lilliu, P. Gao, H.J. Snaith, J. Wang, N.C. Greenham, R.H. Friend, D. Di, Nat. Photonics 12 (2018) 783-789.
[10] Y. Cao, N. Wang, H. Tian, J. Guo, Y. Wei, H. Chen, Y. Miao, W. Zou, K. Pan, Y. He, H. Cao, Y. Ke, M. Xu, Y. Wang, M. Yang, K. Du, Z. Fu, D. Kong, D. Dai, Y. Jin, G. Li, H. Li, Q. Peng, J. Wang, W. Huang, Nature 562 (2018) 249-253.
[11] K. Lin, J. Xing, L.N. Quan, F.P.G. de Arquer, X. Gong, J. Lu, L. Xie, W. Zhao, D. Zhang, C. Yan, W. Li, X. Liu, Y. Lu, J. Kirman, E.H. Sargent, Q. Xiong, Z. Wei, Nature 562 (2018) 245-248.
[12] Q. Wang, X. Wang, Z. Yang, N. Zhou, Y. Deng, J. Zhao, X. Xiao, P. Rudd, A. Moran, Y. Yan, J. Huang, Nat. Commun. 10 (2019) 5633.
[13] F. Zhang, B. Cai, J. Song, B. Han, B. Zhang, H. Zeng, Adv. Funct. Mater. 30 (2020) 2001732.
[14] Y. Liu, J. Cui, K. Du, H. Tian, Z. He, Q. Zhou, Z. Yang, Y. Deng, D. Chen, X. Zuo, Y. Ren, L. Wang, H. Zhu, B. Zhao, D. Di, J. Wang, R.H. Friend, Y. Jin, Nat. Photonics, 13 (2019) 760-764.
[15] S.Y. Lee, S.-H. Kim, Y.S. Nam, J.C. Yu, S. Lee, D.B. Kim, E.D. Jung, J.-H. Woo, S.-m. Ahn, S. Lee, K.-J. Choi, J.-Y. Kim, M.H. Song, Nano Lett. 19 (2019) 971-976.
[16] S.G.R. Bade, J. Li, X. Shan, Y. Ling, Y. Tian, T. Dilbeck, T. Besara, T. Geske, H. Gao, B. Ma, K. Hanson, T. Siegrist, C. Xu, Z. Yu, ACS Nano 10 (2016) 1795-1801.
[17] F. Zhao, D. Chen, S. Chang, H. Huang, K. Tong, C. Xiao, S. Chou, H. Zhong, Q. Pei, J. Mater. Chem. C 5 (2017) 531-538.
[18] H.-K. Seo, H. Kim, J. Lee, M.-H. Park, S.-H. Jeong, Y.-H. Kim, S.-J. Kwon, T.-H. Han, S. Yoo, T.-W. Lee, Adv. Mater. 29 (2017) 1605587.
[19] L. Zhao, N. Rolston, K.M. Lee, X. Zhao, M.A. Reyes-Martinez, N.L. Tran, Y.-W. Yeh, N. Yao, G.D. Scholes, Y.-L. Loo, A. Selloni, R.H. Dauskardt, B.P. Rand, Adv. Funct. Mater. 28 (2018) 1802060.
[20] S. Ternes, T. Börnhorst, J.A. Schwenzer, I.M. Hossain, T. Abzieher, W. Mehlmann, U. Lemmer, P. Scharfer, W. Schabel, B.S. Richards, U.W. Paetzold, Adv. Energy Mater. 9 (2019) 1901581.
[21] J. Wang, C. Song, Z. He, C. Mai, G. Xie, L. Mu, Y. Cun, J. Li, J. Wang, J. Peng, Y. Cao, Adv. Mater. 30 (2018) 1804137.
[22] M.-H. Li, H.-H. Yeh, Y.-H. Chiang, U.-S. Jeng, C.-J. Su, H.-W. Shiu, Y.-J. Hsu, N. Kosugi, T. Ohigashi, Y.-A. Chen, P.-S. Shen, P. Chen, T.-F. Guo, Adv. Mater. 30 (2018) 1801401.
[23] N.J. Jeon, J.H. Noh, Y.C. Kim, W.S. Yang, S. Ryu, S.I. Seok, Nat. Mater. 13 (2014) 897-903.

[24] M. Xiao, F. Huang, W. Huang, Y. Dkhissi, Y. Zhu, J. Etheridge, A. Gray-Weale, U. Bach, Y.-B. Cheng, L. Spiccia, Angew. Chem. Int. Ed. 53 (2014) 9898-9903.

[25] S. Draguta, S. Thakur, Y.V. Morozov, Y. Wang, J.S. Manser, P.V. Kamat, M. Kuno, The Journal of Phys. Chem. Lett. 7 (2016) 715-721.

[26] E. Mosconi, D. Meggiolaro, H.J. Snaith, S.D. Stranks, F. De Angelis, Energy Environ. Sci. 9 (2016) 3180-3187.

[27] W.-J. Yin, T. Shi, Y. Yan, Appl. Phys. Lett. 104 (2014) 063903.

[28] D.-Y. Son, J.-W. Lee, Y.J. Choi, I.-H. Jang, S. Lee, P.J. Yoo, H. Shin, N. Ahn, M. Choi, D. Kim, N.-G. Park, Nat. Energy 1 (2016) 16081.

[29] D. Shi, V. Adinolfi, R. Comin, M. Yuan, E. Alarousu, A. Buin, Y. Chen, S. Hoogland, A. Rothenberger, K. Katsiev, Y. Losovyj, X. Zhang, P.A. Dowben, O.F. Mohammed, E.H. Sargent, O.M. Bakr, Science 347 (2015) 519-522.

[30] W. Xu, Q. Hu, S. Bai, C. Bao, Y. Miao, Z. Yuan, T. Borzda, A.J. Barker, E. Tyukalova, Z. Hu, M. Kawecki, H. Wang, Z. Yan, X. Liu, X. Shi, K. Uvdal, M. Fahlman, W. Zhang, M. Duchamp, J.-M. Liu, A. Petrozza, J. Wang, L.-M. Liu, W. Huang, F. Gao, Nat. Photonics 13 (2019) 418-424.

[31] S.D. Stranks, V.M. Burlakov, T. Leijtens, J.M. Ball, A. Goriely, H.J. Snaith, Phys. Rev. Appl. 2 (2014) 034007.

[32] J.M. Azpiroz, E. Mosconi, J. Bisquert, F. De Angelis, Energy Environ. Sci. 8 (2015) 2118-2127.

[33] T. Leijtens, G.E. Eperon, A.J. Barker, G. Grancini, W. Zhang, J.M. Ball, A.R.S. Kandada, H.J. Snaith, A. Petrozza, Energy Environ. Sci. 9 (2016) 3472-3481.

[34] C. Qin, T. Matsushima, W.J. Potscavage, A.S.D. Sandanayaka, M.R. Leyden, F. Bencheikh, K. Goushi, F. Mathevet, B. Heinrich, G. Yumoto, Y. Kanemitsu, C. Adachi, Nat. Photonics 14 (2020) 70-75.

[35] D.B. Mitzi, J. Mater. Chem. 14 (2004) 2355-2365.

[36] R. Quintero-Bermudez, A. Gold-Parker, A.H. Proppe, R. Munir, Z. Yang, S.O. Kelley, A. Amassian, M.F. Toney, E.H. Sargent, Nat. Mater. 17 (2018) 900-907.

[37] S. Lee, D.B. Kim, J.C. Yu, C.H. Jang, J.H. Park, B.R. Lee, M.H. Song, Adv. Mater. 31 (2019) e1805244.

[38] X. Yang, Z. Chu, J. Meng, Z. Yin, X. Zhang, J. Deng, J. You, J. Phys. Chem. Lett. 10 (2019) 2892-2897.

[39] L.N. Quan, Y. Zhao, F.P. García de Arquer, R. Sabatini, G. Walters, O. Voznyy, R. Comin, Y. Li, J.Z. Fan, H. Tan, J. Pan, M. Yuan, O.M. Bakr, Z. Lu, D.H. Kim, E.H. Sargent, Nano Lett. 17 (2017) 3701-3709.

[40] M. Liu, M.B. Johnston, H.J. Snaith, Nature 501 (2013) 395-398.

[41] J. Burschka, N. Pellet, S.-J. Moon, R. Humphry-Baker, P. Gao, M.K. Nazeeruddin, M. Grätzel, Nature 499 (2013) 316-319.

[42] P. Wang, X. Zhang, Y. Zhou, Q. Jiang, Q. Ye, Z. Chu, X. Li, X. Yang, Z. Yin, J. You, Nat. Commun. 9 (2018) 2225.

[43] C. Li, Y. Pan, J. Hu, S. Qiu, C. Zhang, Y. Yang, S. Chen, X. Liu, C.J. Brabec, M.K. Nazeeruddin, Y. Mai, F. Guo, ACS Energy Lett. (2020) 1386-1395.

[44] A. Dualeh, N. Tétreault, T. Moehl, P. Gao, M.K. Nazeeruddin, M. Grätzel, Adv. Funct. Mater. 24 (2014) 3250-3258.

[45] J.H. Kim, P.W. Liang, S.T. Williams, N. Cho, C.C. Chueh, M.S. Glaz, D.S. Ginger, A.K. Jen,

Adv. Mater. 27 (2015) 695-701.
[46] Y. Liu, I. Shin, I.-W. Hwang, S. Kim, J. Lee, M.-S. Yang, Y.K. Jung, J.-W. Jang, J.H. Jeong, S.H. Park, K.H. Kim, ACS Appl. Mater. Interfaces 9 (2017) 12382-12390.
[47] Z. Xiao, Q. Dong, C. Bi, Y. Shao, Y. Yuan, J. Huang, Adv. Mater. 26 (2014) 6503-6509.
[48] G.E. Eperon, S.N. Habisreutinger, T. Leijtens, B.J. Bruijnaers, J.J. van Franeker, D.W. deQuilettes, S. Pathak, R.J. Sutton, G. Grancini, D.S. Ginger, R.A.J. Janssen, A. Petrozza, H.J. Snaith, ACS Nano 9 (2015) 9380-9393.
[49] Y. Liu, I. Shin, Y. Ma, I.-W. Hwang, Y.K. Jung, J.W. Jang, J.H. Jeong, S.H. Park, K.H. Kim, ACS Appl. Mater. Interfaces 10 (2018) 31366-31373.
[50] Y. Liu, P.M. Hangoma, V. Tamilavan, I. Shin, I.-W. Hwang, Y.K. Jung, B.R. Lee, J.H. Jeong, S.H. Park, K.H. Kim, Nano Energy 61 (2019) 251-258.
[51] J. Liu, J. Leng, K. Wu, J. Zhang, S. Jin, J. Am. Chem. Soc. 139 (2017) 1432-1435.
[52] Q. Shang, Y. Wang, Y. Zhong, Y. Mi, L. Qin, Y. Zhao, X. Qiu, X. Liu, Q. Zhang, J. Phys. Chem. Lett. 8 (2017) 4431-4438.
[53] T. Yin, Y. Fang, W.K. Chong, K.T. Ming, S. Jiang, X. Li, J.-L. Kuo, J. Fang, T.C. Sum, T.J. White, J. Yan, Z.X. Shen, Adv. Mater. 30 (2018) 1705017.
[54] X. Lü, Y. Wang, C.C. Stoumpos, Q. Hu, X. Guo, H. Chen, L. Yang, J.S. Smith, W. Yang, Y. Zhao, H. Xu, M.G. Kanatzidis, Q. Jia, Adv. Mater. 28 (2016) 8663-8668.
[55] A.Z. Chen, M. Shiu, J.H. Ma, M.R. Alpert, D. Zhang, B.J. Foley, D.-M. Smilgies, S.-H. Lee, J.J. Choi, Nat. Commun. 9 (2018) 1336.
[56] D.B. Kim, S. Lee, C.H. Jang, J.H. Park, A.-y. Lee, M.H. Song, Adv. Mater. Interfaces 7 (2020) 1902158.
[57] J. Lim, M.T. Hörantner, N. Sakai, J.M. Ball, S. Mahesh, N.K. Noel, Y.-H. Lin, J.B. Patel, D.P. McMeekin, M.B. Johnston, B. Wenger, H.J. Snaith, Energy Environ. Sci. 12 (2019) 169-176.
[58] H.-H. Fang, R. Raissa, M. Abdu-Aguye, S. Adjokatse, G.R. Blake, J. Even, M.A. Loi, Adv. Funct. Mater.25 (2015) 2378-2385.
[59] X. Gong, O. Voznyy, A. Jain, W. Liu, R. Sabatini, Z. Piontkowski, G. Walters, G. Bappi, S. Nokhrin, O. Bushuyev, M. Yuan, R. Comin, D. McCamant, S.O. Kelley, E.H. Sargent, Nat. Mater. 17 (2018) 550-556.